Czech Technical University in Prague

Faculty of Nuclear Sciences and Physical Engineering

Department of Physics

Study of linear silicon drift detectors of the ALICE detector, selection of detectors appropriate for experiment and completion of detectors.

Research Work

David Tlustý

Supervisor: RNDr. Vojtěch Petráček CSc.
Consultant: Alexander Rashevski, INFN Trieste, Italy

Academic year 2005/2006

Obsah

Část I
Introduction

1 What is ALICE?

ALICE (A Large Ion Collider Experiment) is a general-purpose experiment whose detectors measure and indentify mid-rapidity hadrons, leptons and photons produced in the collision of heavy nuclei, . ALICE is an experiment at the Large Hadron Collider (LHC) optimized for the study in detail the behaviour of nuclear matter at high densities and temperatures, in view of probing deconfinement and chiral symmetry restoration.

The detector consists essentially of two main components:

- the central part - study of hadronic signals and dielectrons
- forward muon spectrometer - study of quarkonia behaviour in dense matter. (Quarkonium is a bound state of quark and its antiquark)

We need to track and identify particles from very low ($\sim$ 100 MeV/c) up to very high ($\sim$ 100 GeV/c) transversal momentum p_T to reconstruct short-lived particles such as hyperons, D and B mesons, and to perform these tasks in and environment with large charged-particle multiplicities, up to 8000 charged particles per rapidity unit at mid-rapidity. In this article we are going to concentrate on an Inner Tracking System (ITS) consisting of six layers of silicon detectors used for tracking. Basic informations about other detectors used in the ALICE one can find in [1], chap. 3.

The basic functions of the ITS are:

1. determination of the primary vertex and of the secondary vertices necessary for the reconstruction of charm and hyperon decays,
2. particle identification and tracking of low-momentum particles,
3. improvement of the momentum and angle measurements of the TPC.

1.1 Tracking in ALICE

We must realize extremely high track density at the LHC. In order to high granularity and a good two-track separation ALICE uses three-dimensional hit information with many points on each track and a weak magnetic field. The ionization density of each track is measured for particle identification.The need for a large number of points on each track has led to the choice of a TPC as the main tracking system. In spite of its drawbacks, concerning speed and data volume, only this device can provide reliable performance for a large volume at up to 8000 charged particles per unit of rapidity. The minimum possible inner radius of the TPC (of about 90 cm) is given by the maximum acceptable hit density. The outer radius (of about 250 cm) is determined by the minimum length required for a $\frac{\mathrm{d}E}{\mathrm{d}x}$ resolution better than 10%. At smaller radii, and hence larger track densities, tracking is taken over by the ITS.

The ITS consists of six cylindrical layers of silicon detectors. The number and position of the layers are optimized for efficient track finding and impact parameter resolution. In particular, the outer radius is the same as the inner of TPC, and the inner one (ITS is the minimum compatible with the radius of the beam pipe (3 cm). **The silicon detectors feature the high granularity and excellent spatial precision required. Because of the high particle density, up to 90 per squared centimeter, the four innermost layers ($r < 24$ cm) must be truly two-dimensional devices**. For this task silicon pixel and silicon drift detectors were chosen. The outer two layers at a radius of about 45 cm, where the track densities are below 1 per squared centimeter, will be equipped with double-sided silicon microstrip detectors. With the exception of the two innermost pixel planes, all layers will have analog readout for particle identification via a $\frac{dE}{dx}$ measurement in the non-relativistic region. This will give the inner tracking system a stand-alone capability as a low-p_T particle spectrometer.

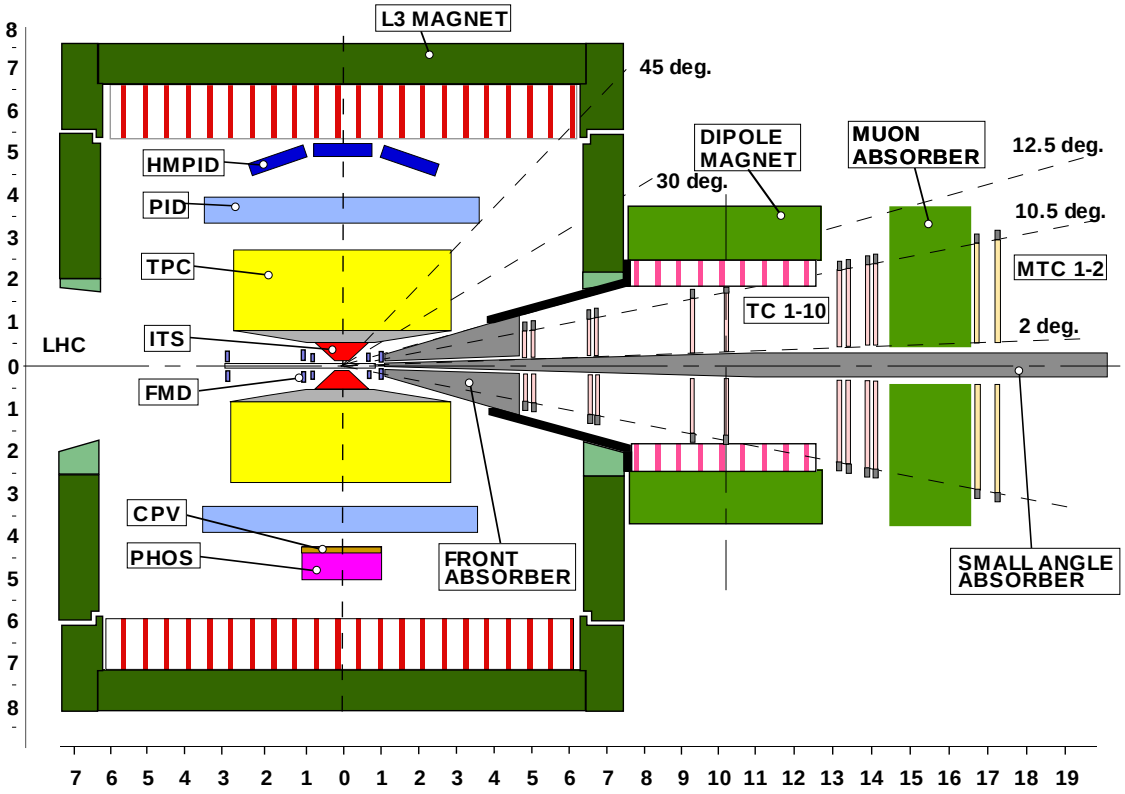

Figure (1): The longitudinal view of complete detector ALICE. It's possible to see how TPC improves the momentum resolution of ITS.

1.2 Physics of the ITS

The ITS will contribute to the track reconstruction by improving the momentum resolution obtained by the TPC. The global event features will be studied by measuring the multiplicity distributions and the inclusive particle spectra. For the study of resonance production ($\rho, \omega and \varphi$) and, more importantly, the behaviour of the mass and width of these mesons in the dense medium, the momentum resolution is even more important. We have to achieve

a mass precision comparable to, or better than, the natural width of the resonances in order to observe changes of their parameters caused by chiral symmetry restoration. Also the mass resolution for heavy states, like $\mathcal{D}$ mesons, J/ψ and Γ, will be better, thus improving the signal-to-background ratio in the measurement of the open charm production, and in the study of heavy-quarkonia suppression. Improved momentum resolution will enhance the performance in the observation of another hard phenomenon, the jet production and predicted jet quenching, i.e. the energy loss of partons in strongly interacting dense matter. The low-momentum particles (below 100 MeV/c) will be detectable only by the ITS. This is of interest in itself, because it widens the momentum range for the measurement of particle spectra, which allows collective effects associated with the large length scales to be studied. In addition, a low-p_T cutoff is essential to suppress the soft γ conversions and the background in the electron-pair spectrum due to Dalitz pairs. Also the PID capabilities of the ITS in the non-relativistic $1/\beta^2$ region will therefore be of great help.

In addition to the improved momentum resolution, which is necessary for the identical particle interferometry, especially at low momenta, the ITS will contribute to this study through an excellent **doublehit resolution** enabling the separation of tracks with close momenta. In order to be able to study particle correlations in the three components of their relative momenta, and hence to get information about the space-time evolution of the system produced in heavy-ion collisions at the LHC, we need sufficient angular resolution in the measurement of the particle's direction. Two of the three components of the relative momentum (the side and longitudinal ones) are crucially dependent on the precision with which the particle direction is known. The angular resolution is determined by the precise ITS measurements of the primary vertex position and of the first points on the tracks. The particle identification at low momenta will enhance the physics capability by allowing the interferometry of individual particle species as well as the study of non-identical particle correlations, the latter giving access to the emission time of different particles.

The study of strangeness production is an essential part of the ALICE physics programme. It will allow the level of chemical equilibration and the density of strange quarks in the system to be established. The measurement will be performed by charge kaon identification and hyperon detection, based on the ITS capability to recognize secondary vertices. The observation of multi-strange hyperons (Ξ^- and Ω^-) is of particular interest, because they are unlikely to be produced during the hadronic rescattering due to the high-energy threshold for their production. In this way we can obtain information about the strangeness density of the earlier stage of the collision. Open charm production in heavy-ion collisions is of great physics interest. Charmed quarks can be produced in the initial hard parton scattering and then only at the very early stages of the collision, while the energy in parton rescattering is above the charm production threshold. The charm yield is not altered later. The excellent performance of the ITS in finding the secondary vertices close to the interaction point gives us the possibility to detect D mesons, by reconstructing the full decay topology.

1.3 Design consideration

1.3.1 Acceptance:

In order to be able to analyse particle ratios, p_T spectra and particle correlations on an event-by-event basis, the tracking system must have a sufficiently large rapidity acceptance. The rapidity coverage of the tracking system ($|\eta|$ <0.9) is large enough to detect several thousand

particles per heavy-ion collision at the currently predicted particle production multiplicity. This rapidity window is also necessary for a good efficiency for detecting the decay of large mass, low transverse momentum particles. An efficient rejection of low-mass Dalitz decays can only be implemented if the detector provides full azimuthal coverage. The first pixel layer has a wider pseudorapidity coverage ($|\eta|$ <1.75) to extend the rapidity coverage of the multiplicity measurement.

1.3.2 d**E**/d**x** measurement:

The ITS contributes to particle identification through the measurement of specific energy loss. To apply a truncated-mean method, a minimum of four measurements are necessary, so four out of the six planes need analog readout. We require the dynamic range of the analog readout to be large enough to provide dE/dx information for low-momentum, highly ionizing particles, down to the minimum momentum for which the tracks have a reasonable (¿ 20%) reconstruction probability.

1.3.3 Material budget:

Multiple scattering effects influence dominantly the momentum and impact parameter resolution for small p_T particles in any existing tracking detector. Therefore the **amount of material in the active volume has to be reduced as much as possible**. However, the thickness of silicon detectors used to measure ionization densities must be approximately 300 μm to guarantee the required signal-to-noise ratio. In addition the detectors must overlap in order to reach full coverage within the acceptance window. Taking also into account the incidence angles of tracks the detectors represent a thickness of 0.4% of X_0. The aim set in the ALICE technical proposal was to reduce the thickness of the additional material in the active volume, i.e. electronics, cabling, support structure and cooling system, to a comparable effective thickness. The current design tries to meet this challenge. As shown in Chapter 5 of [2], the resulting relative momentum resolution is better than 2% for pion momenta between 100 MeV/c and 3 GeV/c.

1.3.4 Spatial precision and granularity:

The granularity of the detectors in the ITS is dictated by the track densities expected. The system is designed for a maximum track density of 8000 tracks per unit of rapidity, the upper limit of the current theoretical predictions. Therefore up to 15 000 tracks will have to be detected simultaneously in the ITS. Keeping the occupancy of the system at the level of a few per cent requires several million effective cells in each layer of the ITS. The resolution of the impact parameter measurement is determined by the spatial resolution of the ITS detectors. For charmed particles the impact parameter resolution must be better than 100 μm in the rφ direction. Therefore the ITS detectors have a spatial resolution of the order of a few tens of μm, with the best precision (12 μm) for the detectors closest to the primary vertex. In addition, for momenta larger than 3 GeV/c, relevant for the detection of the decay products of charmed mesons and high-mass quarkonia, the spatial precision of the ITS becomes an essential element of the momentum resolution. This requirement is met by all layers of the ITS with a point resolution in the bending plane about one order of magnitude better than that of the TPC, which in turn provides many more points.

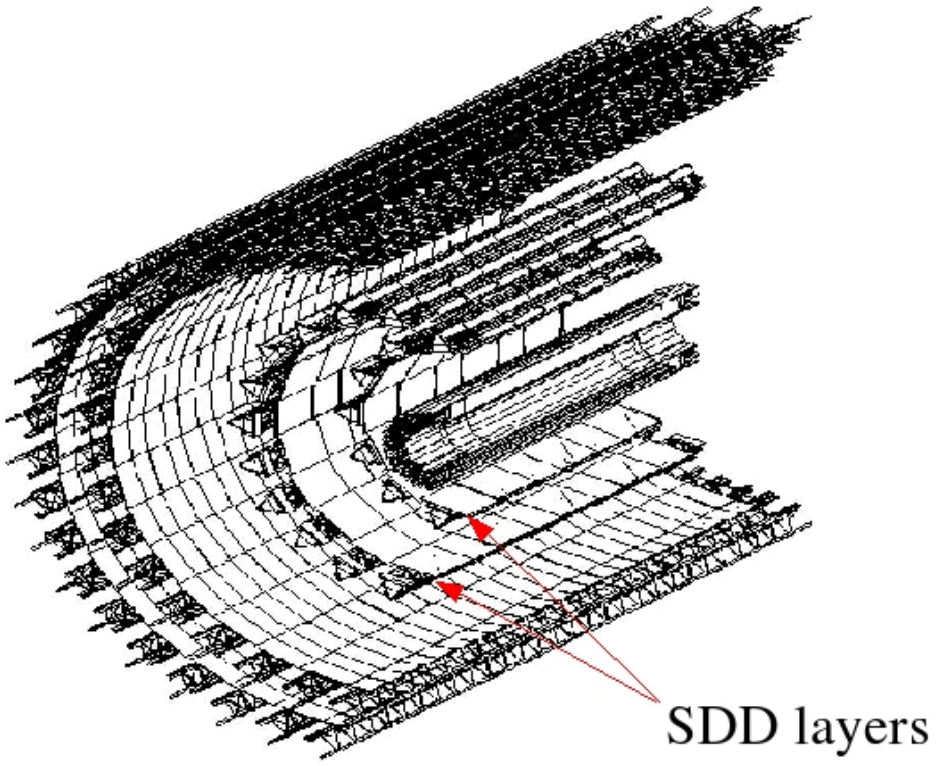

Figure (2): SDD layers in ITS

1.3.5 Readout rate:

The ALICE system will be used in two basically different readout configurations, operated simultaneously with two different triggers. The centrality trigger activates the readout of the whole of ALICE, in particular all layers of the ITS, while the trigger of the muon arm activates the readout of a subset of fast readout detectors, including the two inner layers of the ITS. Therefore the readout time for the pixel detectors is set at 400 μs.

Část II
TECHNICAL DESCRIPTION OF SILICON DRIFT DETECTORS OF THE ALICE EXPERIMENT

2 Introduction.

The Inner Tracking System (ITS) - see fig 2 of the ALICE experiment at LHC will consist of six cylindrical layers of high precision position-sensitive detectors. 260 identical silicon drift detectors (SDDs) will equip the 3rd and the 4th layer, providing position information in two dimensions and dE sample. This part describes the detector and gives its geometrical and

electrical specifications.

3 General detector characteristics.

3.1 Material.

Special care should be dedicated to the starting material. Doping fluctuations can cause distortions in the drift trajectories and deteriorate significantly the position resolution of the detector. Hence, highly homogeneous material is needed. The detectors are fabricated on $5-inch$ diameter, neutron transmutation doped (NTD)[1] , silicon wafers with a resistivity of about $3k\Omega \cdot cm$ and a thickness of 300 μm. NTD silicon suitable for the production of SDDs should have doping maximum variations of less than 6%.

3.2 Basic SDD structures.

The design of most of the modern linear SDDs necessarily presents the following structures:

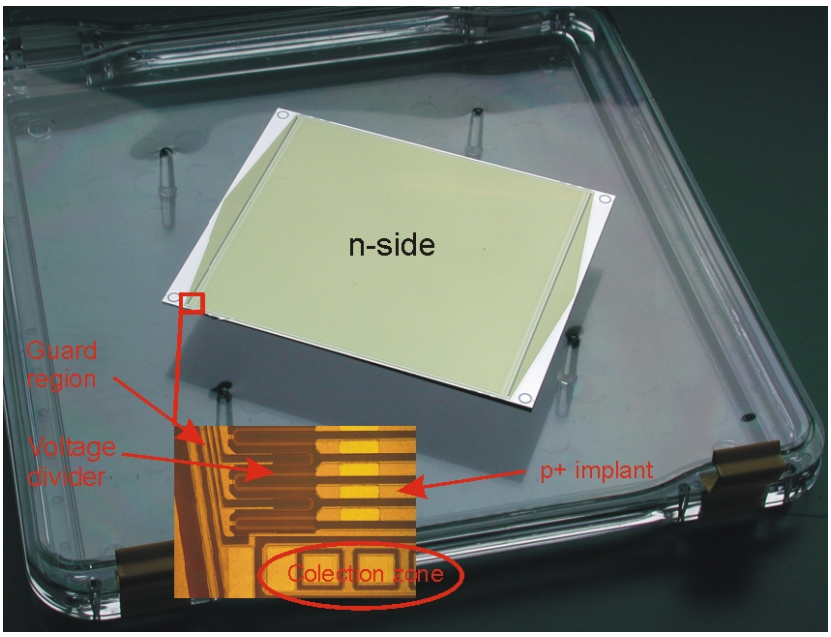

a series of parallel drift cathodes (p^+ implant strips in the case of n-type silicon substrate) is deposited on both sides of the detector, first, to fully deplete its volume and, second, to provide a constant electrostatic field parallel to the wafer surface, forming a drift region. Drift cathodes are biased through a high voltage divider. In a large scale application of SDDs it is important to minimise the number of external connections to the detector, thus, it is very desirable to integrate the high voltage divider in the detector substrate. This can be done with

[1]Semiconductor materials which have been doped by neutron transmutation require annealing at high temperatures in order to alleviate radiation damage and to restore electrical resistivity; however, the minority carrier lifetime is reduced significantly through the irradiation and/or the annealing process. A method for increasing the minority carrier lifetime while maintaining the restored electrical resistivity is achieved by cooling the heated annealed materials at a cooling rate less than about 4.degree. C. per minute and preferably less than about 3.degree. C. per minute to ambient temperatures.

high resistivity p^+ implantations or polysilicon resistors (fig 4). Guard cathodes connected with a certain pitch to the drift cathodes serve to scale gradually the high potential of the drift cathodes down to the ground potential of the n^+ ring at the detector edge. Usually, some of the last drift cathodes closest to the anodes are externally biased and serve to bring drifting charges effectively from the middle plane of the detector towards the surface where they are collected by an array of n^+ anodes. Normally, this part of the drift region is referred to as the 'collection zone'. Conventionally, the anode side of the SDD is called n-side (as only this side presents n^+ implantations) and the other side is called p-side. The drift velocity $\mathbf{v_d}$ in the SDD is very sensitive to temperature variations in the silicon substrate (about 1%/K). Mobillity was measured [4]

$$\mathbf{v_d} = \mu\mathbf{E}, \qquad \mu(T) = \mu(300)\left(\frac{T}{300}\right)^{-r} \tag{1}$$

where coeficient $r = -2.3$ was measured and $\mathbf{E}$ is intensity of electrical field.

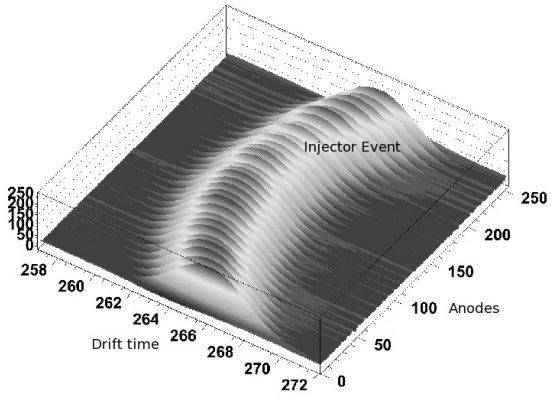

The current flowing in the integrated high voltage divider causes heat dissipation which gives rise to certain temperature gradients in the sensitive region of the SDD. That is why it is very important to have a way to monitor 'on-line' the drift velocity across the sensitive area in order to calibrate the drift time for temperature variations. This can be accomplished with a suitably designed structure of charge injectors (infrared laser, n-type implants or MOS capacitors) - see fig. 5. In the fig. on the left we can see the result of measuring the space charge distribution from injector event. In the middle of the detector (anodes 100 - 150) we see that the detector is colder so that drift speed is higher.

3.3 Detector geometry.

For main view of the detector geometry see fig (6)

The detector is symmetrical with respect to the central p^+ cathode, i.e. it has a bi-directional structure, where electrons drift in direction from the central p^+ cathode towards two linear arrays of n^+ anodes. Even though the silicon pad containing the detector is cut from the wafer as a rectangle with an area of $87.6 \times 72.5 mm^2$, the detector itself has a hexagonal shape with a rectangular sensitive area. The rectangular sensitive area allows to minimise the overlapping of adjacent SDDs in the ladder assembly, while the rectangular shape of the pad containing the detector provides the sensitive area with a one-dimensional distribution (across the drift direction) of the heat dissipated by the integrated voltage divider. Indeed, resistors of the integrated voltage divider connect drift cathodes at the flanks of the sensitive area and are aligned in two columns along the drift direction. For each half-detector there are 292 drift cathodes with a pitch of $120\mu m$ and (256+2) anodes with a pitch of $294\mu m$. So, the length of the sensitive area delimited by two arrays of anodes is $70.0mm$, while the width of the sensitive area along the anodes is $75.3mm$. The sensitive-to-total-area ratio is

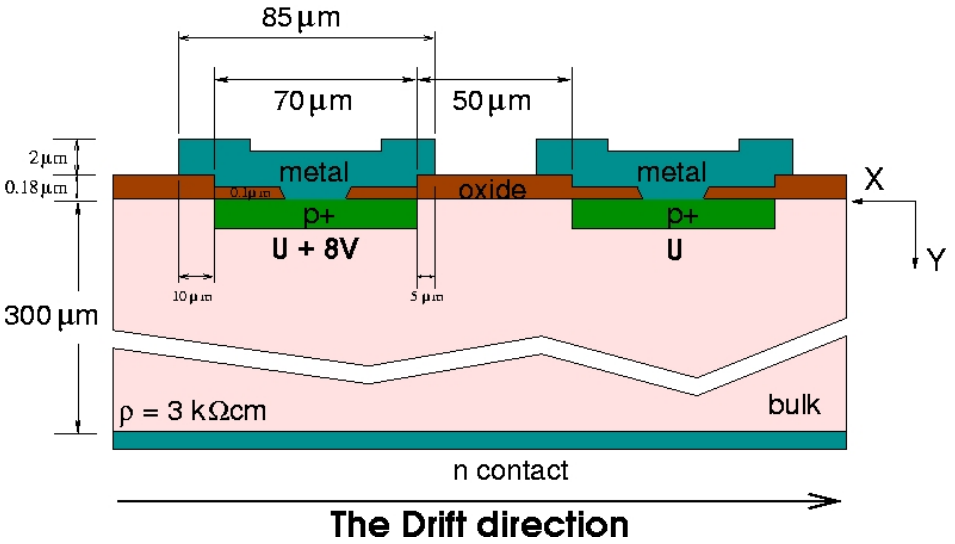

Figure (3): SDD cut, p+ implants on n-type Silicon semiconductor

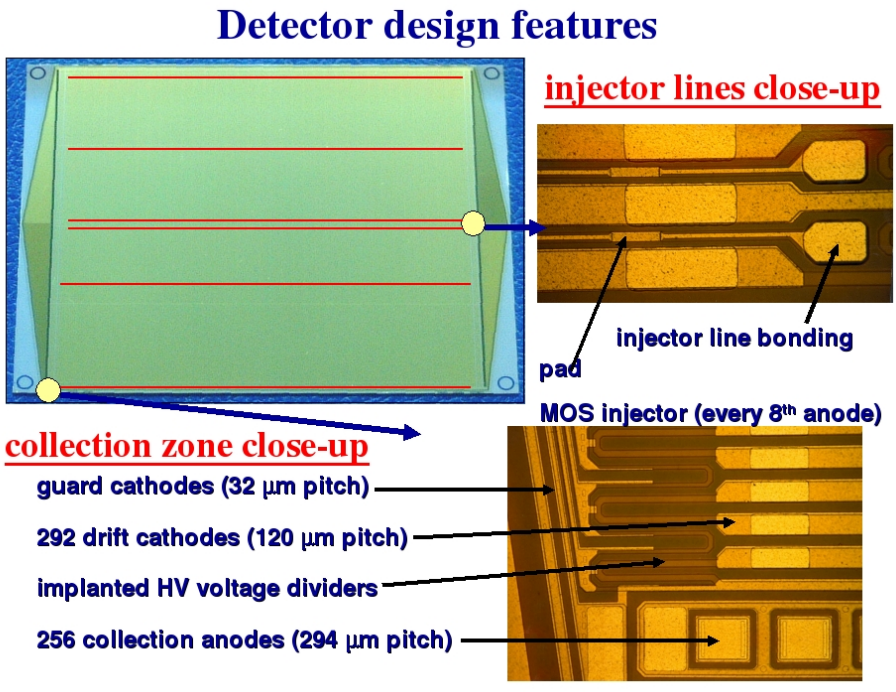

Figure (4): Overview of SDD structure

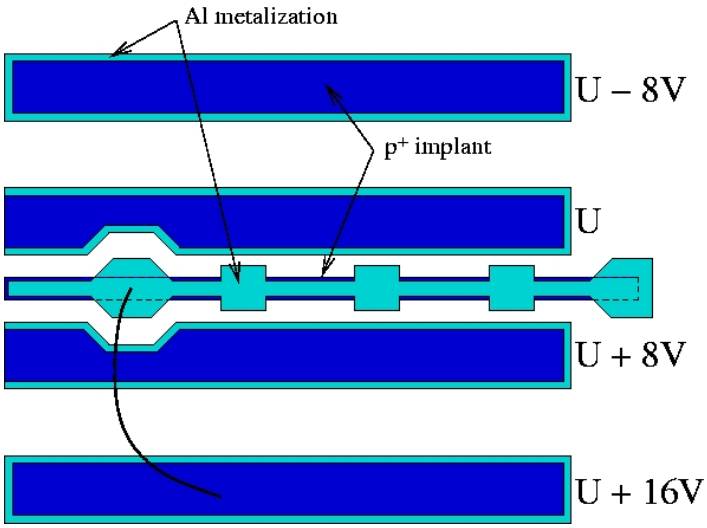

Figure (5): Design of the injector and its bonding

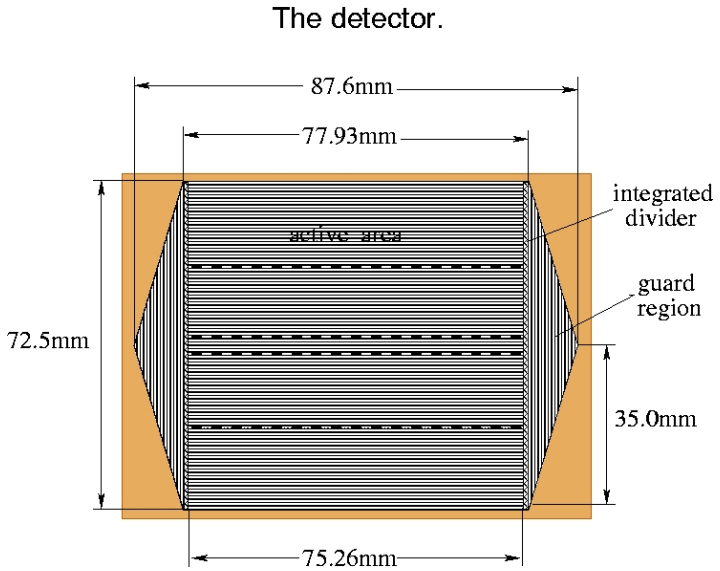

Figure (6): Detector geometry

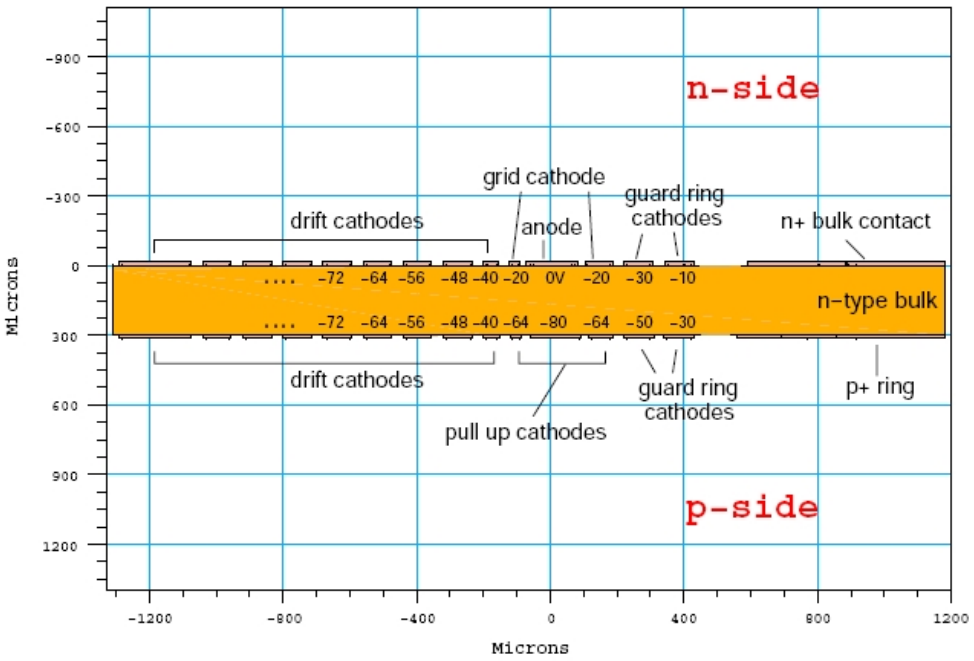

Figure (7): Cut of the colection zone with with 'kick up' cathodes on the p-side

88% (considering the detector itself, not the rectangular pad containing the detector). Aside of the integrated dividers there are two triangular areas constituted by the guard p^+ cathodes. There is one guard cathode every two drift cathodes, so the potential difference between adjacent guards is twice that between adjacent drift cathodes. The pitch of the guard cathodes is $32\mu m$. In the following see fig (4) and (5)

The collection zone of the detector consists of only 3 cathodes biased independently from the integrated voltage divider: the 'grid' cathode on the n-side separates anodes one from another, while two 'kick up' cathodes on the p-side force the drifting charge towards the anodes array, fig (7). One 'kick up' cathode is placed in front of the array of anodes, while the second 'kick up' cathode surrounds the first one. The potential distribution is placed on the fig. (8).

The integrated divider of the n-side ends with a bonding pad $100\mu m$ away from the bulk contact (n^+ ring implanted along the detector edge), while the integrated divider of the $p-$side is closed to the p^+ ring implanted along the detector edge.

To monitor the drift velocity across the sensitive area and to calibrate the drift time for temperature variations, 'point-like' MOS charge injectors are implemented. In each half-detector three arrays of injectors are realized on both $n-$ and $p-$side at distances of $5mm$, $17.6mm$ and $34.0mm$ from the anodes. The injector pitch is $2.35mm$ (every eight anodes).

3.4 Electrical conditions.

The detector is planned to work at a potential difference of about $8\,V$ between adjacent drift cathodes which corresponds to a drift field of $670\,V/cm$.

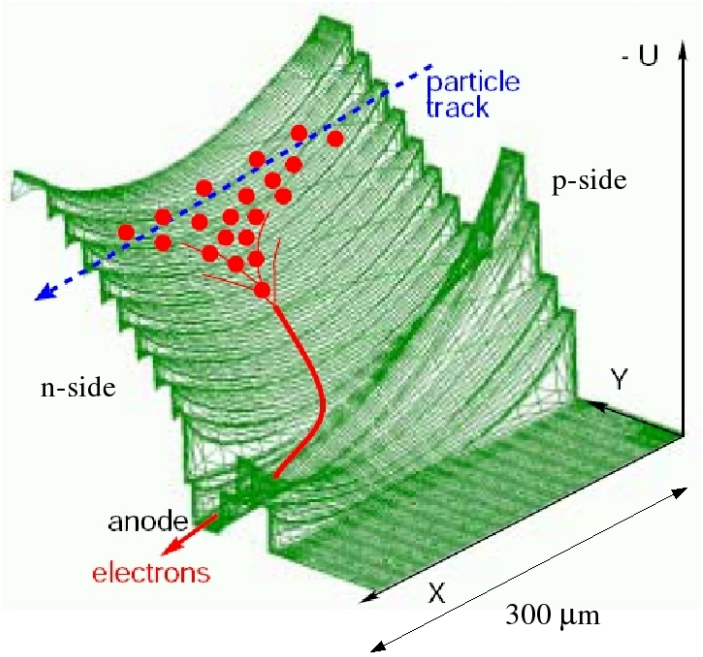

Figure (8): Potential distribution of the colection zone

3.4.1 Operational stability

Designing a SDD without an external divider, one of the keystones is to ensure its long-term electrical stability. It is known, that the leakage and punch-through currents flowing in a silicon detector can be very dependent on the environmental conditions, if one does not foresee special solutions in the detector design to attenuate this influence. From this point of view, in case of the SDD, the punch-through phenomenon is the most critical. When the voltage difference between adjacent p^+ cathodes reaches a critical value U_{pt} , a hole current starts to flow. This phenomenon can be considered as a parasitic resistor inserted in parallel to the implanted resistor of the divider, altering, thus, the linear potential distribution on the cathodes. Under certain conditions the negative charges coming from the environment do not only partially or completely compensate the positive charge inside the oxide, but starts to prevail and causes the formation of an inversion layer under the oxide. Consequently, the value U_{pt} can decrease in a dramatic way, and the seemingly perfect linearity of the potential distribution on the drift cathodes, measured a short time after having biased the SDD, becomes altered on a longer time scale. This decrease of U_{pt} can take hours and even days before reaching an asymptotic limit. In the silicon drift detector the guard cathodes are usually most exposed to the punch-through phenomenon. It is necessary to ensure an asymptotic limit higher than $20V$ for a described above geometry of the guard structure.

3.4.2 Integrated voltage divider

The resistor values of the integrated divider are constant till the drift cathode ♯291 (that is the last drift cathode before the 'grid' cathode on the n-side and the last drift cathode before the 'kick up' cathodes). On the n-side there are two p^+ ring cathodes beyond the anode array. These cathodes are connected in series, via integrated resistors, to the cathode ♯291 and, at

the other end, to the bonding pad $100\mu m$ away from the bulk contact (n^+ ring implanted along the detector edge). In the mounted detector this pad is wire connected to the bulk contact to be grounded. The integrated resistors for these cathodes are chosen in a way that the cathode ♯292 has 3/4 of the potential of the cathode ♯291, while the cathode ♯293 has 1/2 of the potential of the cathode ♯292. On the p-side there are two p^+ ring cathodes beyond the 'kick up' cathodes: the cathode ♯292 is connected to the cathode ♯293 and the cathode ♯293 is connected to the p^+ ring implanted along the detector edge via integrated resistors. There is an interruption in the integrated divider of the p-side between the cathode ♯291 and the cathode ♯292 in order to have the possibility to perform IV-measurement of all cathodes as a unique diode. In the mounted detector the cathode ♯292 is wire connected to the cathode ♯291. The integrated resistors for these cathodes are chosen in a way that the cathode ♯293 has 3/4 of the potential of the cathode ♯291.

4 Technical Specifications.

Silicon substrates, with the following characteristics, is provided by the producer:

- diameter: $127\,mm$ $(5\,inch)$;
- doping: Neutron Transmutation Doping (n-type Phosphorous);
- resistivity: $2k\Omega \cdot cm < \rho < 4k\Omega \cdot cm$;
- maximum doping variations per wafer: < 6 %;
- crystal plane orientation: (100) or (111);
- thickness: $300 \pm 15\mu m$;
- polishing: polished on both sides;

The number of wafers depends on the final production yield of the detectors. The detector that passes the requirements as outlined in enclosure "Testing and inspection" is considered "known to be good". The required number of these detectors is 280.

Both sides of the detector are covered by a passivation layer, whose purpose is to provide electrical insulation of metal features and to help protecting the device from possible mechanical damage and from contamination during testing, assembly and operation. Suitable openings in the passivation layer allow probing and/or bonding on the individual strips, and on the substrate all along the edge of the detector. Passivation material is polyimide.

The test structures on the wafer is used for measurement of the parameters specified in the test specifications.

Each detector is diced from the wafer as a pad with dimensions specified in Subsection: Geometric Specifications.

5 Design Specifications.

5.1 Mask Layers.

Here is the minimum indispensable list of masks of the detector:

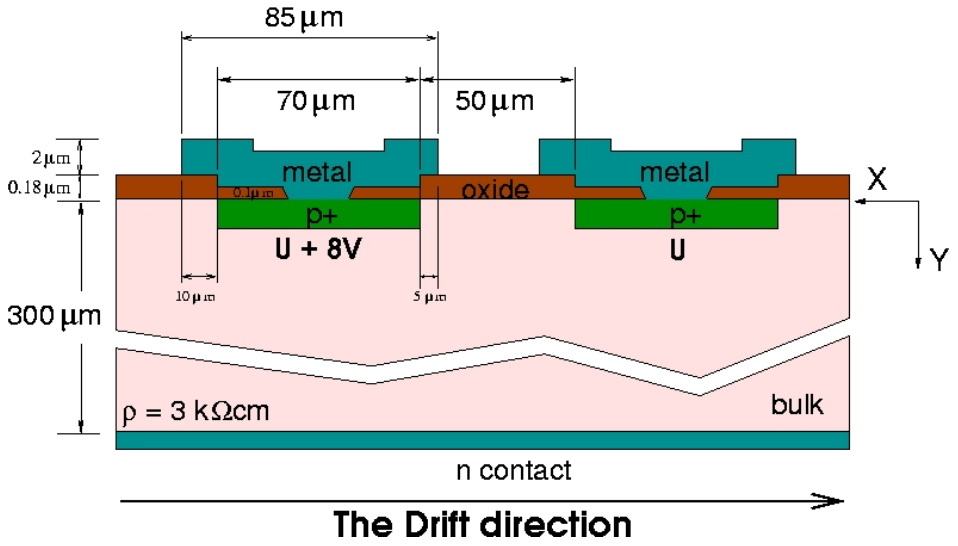

Figure (3: SDD cut, p+ implants on n-type Silicon semiconductor

- Mask ♯1: Boron implant on p-side;
- Mask ♯2: Boron implant of integrated divider on p-side;
- Mask ♯3: Boron implant on n-side;
- Mask ♯4: Boron implant of integrated divider on n-side;
- Mask ♯5: Phosphorus implant on n-side;
- Mask ♯6: Aluminium mask for p-side;
- Mask ♯7: Aluminium mask for n-side;
- Mask ♯8: Passivation mask for p-side;
- Mask ♯9: Passivation mask for n-side;

5.2 Geometric specifications.

Tolerances on the cut with respect to the external guard rings of the detector are explicitly indicated. Tolerances on the sizes and relative positions of internal features depend on the processing equipment available to the manufacturer and on the fabrication technology adopted.

In any case, mask overlay accuracy should be within $\pm 1 \mu m$. Front-to-back alignment of the detector geometries should be within $\pm 5 \mu m$.

On either side the design of the detector is symmetrical with respect to the central drift cathode. The drift, guard and injector structures are identical for both n-side and p-side, while the design of the collection zone is different for n-side and p-side. Only n-side presents n^+ implantation (collecting anodes and n^+ bulk contact which is implanted as a ring along the detector edge):

See fig (3).

- Nominal size of the cut detector: $87.6mm \times 72.5mm = 6351mm^2$
- Overall width and tolerance: $87600 + 25 - 25\mu m$
- Overall length and tolerance: $72500 + 25 - 25\mu m$
- Nominal position of the cut border:
  - along the anodes: centered with respect to the symmetry of the drift strips.
  - along the drift direction: centered with respect to the structure of the guard rings.
- Tolerance on each cut edge: $25\mu m$ out-wards of the nominal position, $25\mu m$ in-wards.
- Sensor thickness: $300 \pm 15\mu m$
- Sensor Flatness: $\pm 5\mu m$ on each side of the same detector
- Parallelism error ('taper'): $\leq 10\mu m$ on any dimension of the detector
- Distortion ('warp'): $\leq 20\mu m$
- Active surface: determined by the number, pitch and length of the drift strips (see below), that is $75.3mm \times 70mm = 5271mm^2$
- Drift strip pitch: $120\mu m$
- Implant width of the drift strip: $70\mu m$.
- Metallization width of the drift strip ensure adequate values for the electrical parameters, in particular to keep the electric stress at the implant border below the critical value and to avoid the punch-through between the strips (see enclosure "General detector characteristics").
- Metallization is DC connected to $p+$ implant via periodically placed apertures ($10\mu m \times 10\mu m$) in the oxide.
- Guard strip pitch: $\leq 32\mu m$.
- Implant and metallization width of the guard strip ensure adequate values for the electrical parameters, in particular to keep the electric stress at the implant border below the critical value and to avoid the punch-through between the strips (see enclosure "General detector characteristics").
- Drift strip length: adequate to ensure full charge collection on 256 anodes, that is $> 75600\mu m$.
- Number of drift strips on one side: 583.
- Bonding pads of drift strips: 6 pads for each drift strip; 2 pads are located near each end of a full-length metal strip (second pad put $1mm$ from the first pad inside the strip); 2 pads are located in the middle of a full-length metal strip (separated $1mm$ one from another).

- Dimensions of bonding pads: rectangular shape with round corners, $200\mu m$ long $\times 70\mu m$ wide (referring to opening in the passivation layer).
- Number of p^+ guard rings on n-side beyond the anodes: 2 (see enclosure "General detector characteristics").
- Number of p^+ guard rings on p-side beyond the 'kick-up' strips: 2 (see enclosure "General detector characteristics").
- Number of anodes: 256 + 2.
- Anode pitch: $294\mu m$.
- Anode size as n^+ implant: $(150 - 170)\mu m$ (along the anode array) $\times(110 - 130)\mu m$ (along the drift direction).
- Anode size as Aluminium metallization: $(180-200)\mu m$ (along the anode array) $\times(130-150)\mu m$ (along the drift direction).
- Size of bonding pads for anodes: is equal to metallization size.

There are text and optical markers on the detector to ease testing of the detectors and assembly of detector modules, such as:
Strip number identification;
Mechanical positioning reference marks;

6 Testing and Inspection.

On the contrary to the silicon microstrip or pixel detectors where possible locally bulk or surface generated high current is confined within few strips/pixels, a similar defect in the SDD is propagated throughout the whole detector. Normally, few percent of strip/pixels with high current are included in the acceptance requirements for these detectors. This is not the case of the SDD, where a single local defect generating high current can make the whole detector unusable. Another feature of silicon drift detectors is that they have p+ implantation on both n- and p-side, that is both of them are junction sides. The operating voltage for the ALICE silicon drift detector is $-2400V$ applied to the strips $\sharp 0$ of n-side and p-side. The n^+ bulk contact at the detector edge is put to ground. But it does not mean that this bias is applied to the p-n junctions of the detector. Indeed, the junctions are biased at the voltage equal to the depth of the potential gutter created between two sides of the silicon drift detector. For a detector produced on $300\mu m$ thick silicon wafer with a resistivity of $3\,k\Omega cm$ the value of the potential gutter depth is about $30V$. The exception is the collection zone where 'kick up' cathodes are biased at higher potentials that the depth of the potential gutter.

6.1 Visual inspection.

Visual inspection was carried out to find processing flaws. All wafers were inspected thoroughly in a microscope. The inspection was performed to find the defects listed in the following subsections.

6.1.1 Defect Definition.

Bridge : the distance to the neighbouring pattern is reduced to less than 50% of the design distance;

Interruption : the width of a structure is at some point reduced to less than 50% of the design width;

6.1.2 Areas for visual inspection.

The following areas of both n-side and p-side of the detector were visually inspected:

Cathode area :
No bridges between Boron implants allowed (if the oxide thickness permits to see them).
No bridges between Aluminium lines allowed.
No interruption of Aluminium lines allowed.

Injector lines :
No bridges in Boron implants of Aluminium lines to surrounding patterns allowed.
No interruption of Aluminium lines allowed.

Anodes (only on n-side) :
No bridges in Phosphorus implants to surrounding Boron implant of the 'grid' cathode allowed.
No bridges in Aluminium to surrounding metal of the
'grid' cathode allowed.
All anodes must be covered with Aluminium.

Resistors of integrated voltage divider :
No interruption allowed (if the oxide thickness permits to see them).

Guard area :
No bridges between Boron implants allowed (if the oxide thickness permits to see them).
No bridges between Aluminium lines allowed.
No interruption of Aluminium lines allowed.

Cut area :
The quality of the cut line should satisfy the tolerances on the cut listed in enclosure "Geometric specifications".

6.2 Electrical parameters measured on test structures.

The measurements were performed at $20\,^oC$ The following parameters were measured on test structures:

Oxide charge density .
Fixed oxide charge density Q_{ox} derived from the flat-band voltage measurements on MOS test structures should be less than $6 \times 10^{11} q/cm^2$. The flat-band voltage was measured in 4 different points both on n-side and p-side of the wafer. The most suitable areas to place 4 MOS test structures both on n-side and p-side are 4 triangles that

together with the hexagonal detector complete the silicon rectangular pad cut from the wafer (see enclosure "General detector characteristics").

Capacitance-Voltage Measurements .
CV-measurements were performed on one test diode of each wafer to control the doping concentration. This is not an acceptance criterion for the detectors, but is measured to control the resistivity of the wafers.

Current-Voltage Measurements .
IV-measurements were performed on test diodes of each wafer. Both direct and reverse current were measured.
The direct current should be more than $1\,mA/cm^2$ at $1V$.
The reverse current should be less than $50nA/cm^2$ at the full depletion voltage.

Resistors of integrated voltage divider .
The resistors were measured on test structures with a bias resistor chain with 10 resistors. Four test structures were measured on each side of the wafer.

- Value of one resistor $140 - 200\,k\Omega$;
- Maximum variations of the resistor values from the average value measured on a production batch $\leq \pm 20\%$;
- Maximum variations of the resistor values from the average value measured on one detector $\leq \pm 3\%$.

6.3 Current-Voltage Measurements on the detector.

A preliminary IV-measurement was performed by INFN Trieste group, where I participated. It gave indications about the currents in the detector under the working bias voltage. This is possible since all drift cathodes are connected together through the integrated voltage divider. Two probes are enough to bias the whole cathode chain of one side: the first probe is put to the last cathode and the second one is put to the bulk contact. This measurement have been done for both n-side and p-side of the detector. The leakage current is measured up to a bias voltage of -80V, even though the working value referred to the bottom of the potential gutter is around $-30V$ (for a resistivity of $3k\Omega \cdot cm$). It is required that at $-30V$ the current is less than $5\mu A$. Note: in case of p-side it was necessary to use the third probe to put the cathode ♯292 in order to avoid the punch-through between the cathode ♯291 and the cathode ♯292. The measurements were performed at $20\,^oC$

6.4 Single anode Current Measurements.

The detectors pre-selected with the IV-measurements were tested using a double sided probe station which is about to be installed in Trieste. Single anode currents were measured at a bias voltage of $-2500V$, that is the working bias voltage plus a safety margin of $100V$. The measurements were performed after having kept each detector at the detector at the bias voltage of $-2500V$ for 2 hours. Each detector should not have more than 2% of the anodes with a current higher than $100nA$. In addition, the average current per anode should be less than $10nA$, without taking into consideration the 'hot' anodes with a current higher than $100nA$. The measurements were performed at $20\,^oC$.

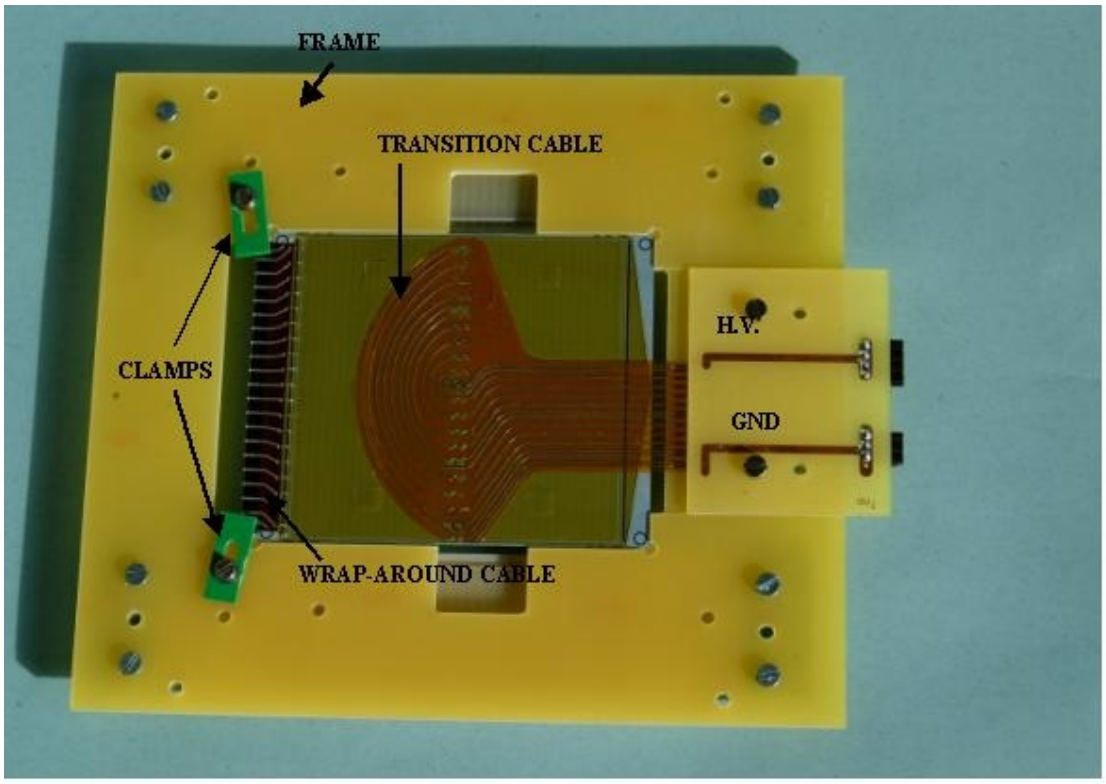

Figure (9): Completly tested and assembled detector in the frame. The detector is prepared to send to Torino.

6.5 Voltage measurements on the integrated voltage divider

The detectors that passed succesfully the single anode current test, proceeded to the measurement of the voltage distribution on the drift cathodes (both n-side and p-side) at the potential bias of $-2400V$. Using the double sided probe station, the voltage drops between ten consecutive drift cathodes were measured. The maximum peak-to-peak variation of the voltage drop distribution on one side of a half-detector should not be more than $5V$. The measurements were performed at $20\,^oC$.

7 Completation of tests-passed detector

After qualification procedure was done the accepted detectors were assembled with HV bias microcables in two sites:
Instituto Nazionale di Fisica Nucleare - Trieste - Italy
and
Ohio State University - Columbus - USA (grade B SDDs)
I participated in Instituto Nazionale di Fisica Nucleare - Trieste - Italy.

To receive the result on fig. (9) it's necessary to follow the **Route for HV microcables assembling onto SDD**

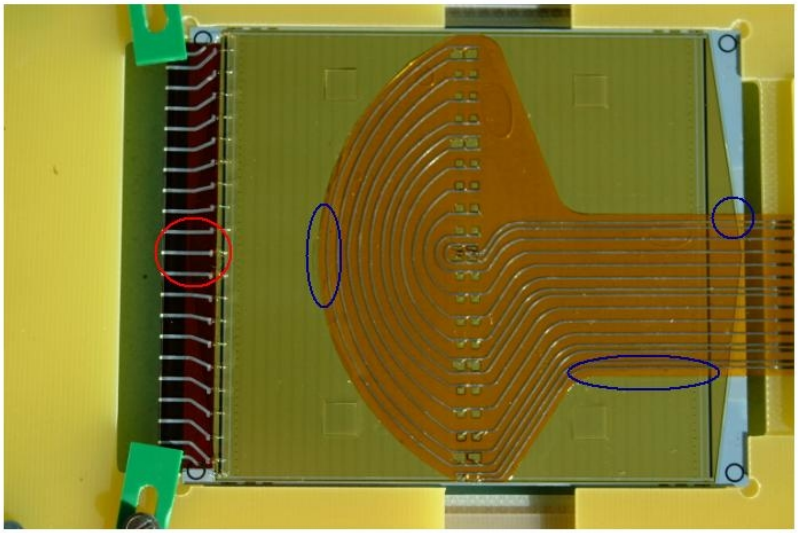

Figure (10): The detector with wrap-around and transition cable with marked areas which are most critical

- Wrap-around cable gluing (30 min), cure 4 hours at 60°C
- Wrap-around cable bonding on p-side and n-side (20 min)
- Gluing on p-side of Transition cable and 4 glass rectangulars (1 hour), cure 4 hours at 60°C
- Transition cable bonding (20 min)
- Mounting the assembly onto the frame for shipment to Torino (10 min)
- Glue passivation of bonds on Transition and wrap-around cables (30 min), cure 4 hours at 60°C
- Shipment of ready assemblies from Trieste to Torino

Totaly: 3 hours of manual operations and 12 hours heat cure.

7.1 Electrical test on assembly "SDD + wrap-around microcable + transition microcable

Most critical areas from the point of view of the electrical stress are delimited in red and blue, see fig. (10). Assembly survived 100 h exposition to a bias voltage of -2370 V. Glue protection of critical areas plays a very positive role in increasing the electrical robustness of the assembly. In critical areas delimited in blue the distance between the traces and the edge of Transition cable had to be increased from 1 mm to 3 mm.

7.2 Completion step by step

Main purpose of transition cable is to bias every 30th. cathode and so precize the voltage distribution on the detector. Wrap-around cable only conects p-side with n-side of the detector.

1. **Preparing of the glue:** To glue Transition and Wrap-around cables onto SDD as well as to protect wire bonds between SDD and cables, High Strength Transparent Silicone Rubber Compound RTV 615 was chosen. This glue is highly recommended by industry with rich experience of using it for silicon sensors assembles. It has low viscosity - easily penetrates in very narrow gaps, avoiding air bubles, it's transparent so that it's easy to control of bonds in post-treatment assembly. And it's rubber like, never becomes rigid - no mechanical stress to silicon substrate.

To prepare the glue I needed chemical weights because to make the glue solid there was requirement of high accuracy in mixing two compounds of the glue, strictly 1:10. During the mixing a lot of bubbles originated. To remove them I put the glue to vacuum and let it there for 15 minutes. After that the glue was prepared.

2. **Putting the glue into wrap-around cable:**

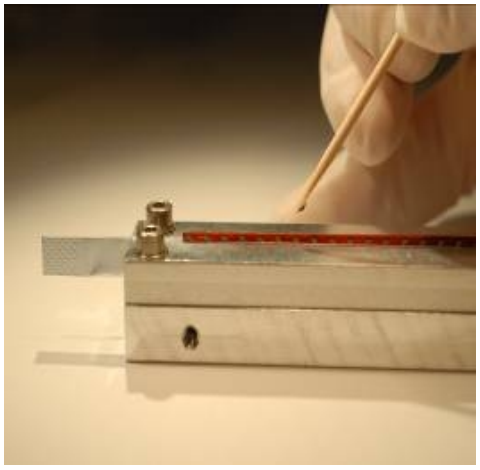

To put the appropriate amount of glue the holder for the cable was needed. During the inserting of the wrap-around cable into the holder I had to manipulate with cable carefully to avoid scratches on metalic parts of the cable. When the cable had been in the holder I started put the glue with wooden stick into the cable.

Here it is possible to see, how the glue have been puted into the wrap-around cable. The amount of glue must be appropriate to avoid the glue overflow on the detector area and cover bonding points.

3. **Positioning the wrap-around cable on the detector**

The wrap-around cable should be positioned on the detector so that metalic parts (where are bonding points) are closest into bonding points on the detector.

4. **Securing and curing**

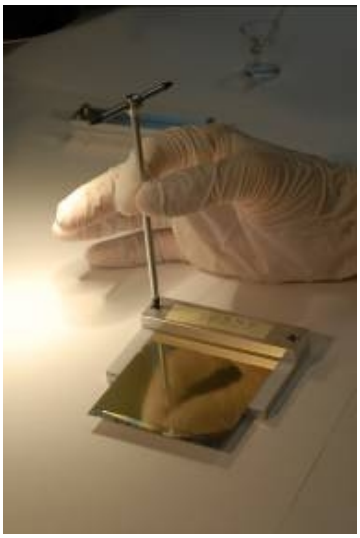

To let the glue heat curing, the wrap-around cable on the detector and the detector in the holder fixing was needed. Then it was possible to put the holder with detector into an owen at 60°C, see picture below

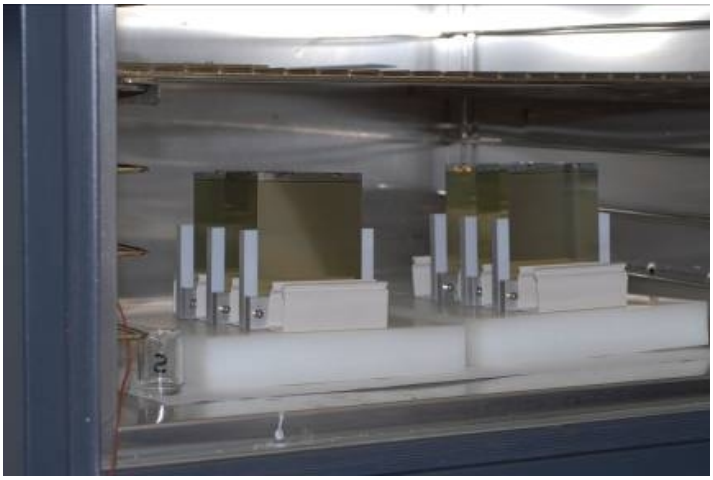

5. **Wrap-around cable bonding**

The detector with glued wrap-around cable is possible to bond. We have used technology *Ultrasonic wedge bonding with aluminum wires* - see supplement "Wire bonding". On the picture is detector fixed to rest by air pump and wedge needle. This operation is the most exacting process at accuracy and care.

6. **Putting the glue on a transition cable**

   Before putting glue on a transition cable is necessary to control the quality of the cable. As we mentioned above in some places of the detector there is diference between potentials to 2370 V on length smaller than 1 mm. Every depletion can cause impalement of dielectrical stronghold.

   After that control was used a pneumatical feeder to put uniform drops of glue on the transition cable.

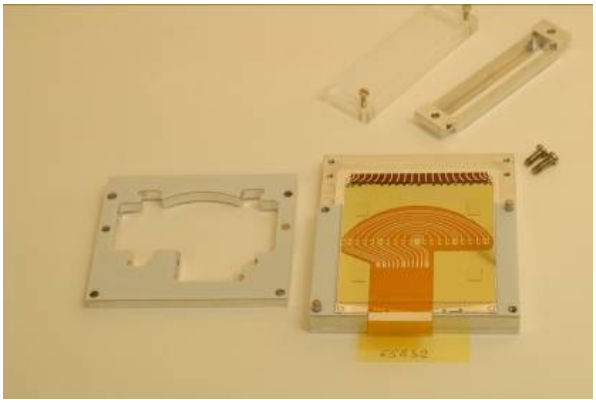

The transition with glue must be positioned on the detector precisely. This secures a special holder which is on the picture. Then is very important to remove all air bubbles (originated during putting the trans. cable on the detector) from the space between the cable and the detector. Anyway there is also risk of impalement because on the surface of an air bubble the electrical field increases. After that I glued four glass rectangulars on four given places on the detector. These rectangulars is used for fixing the detector on the ladder (as mentioned in the introduction). Then the detector is prepared to put into the owen for head curing, picture below.

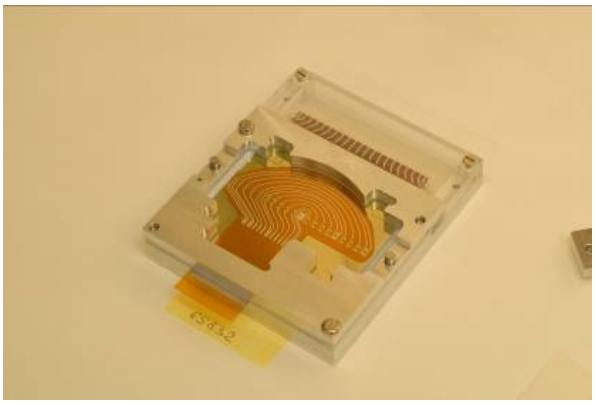

7. **transition cable bonding**

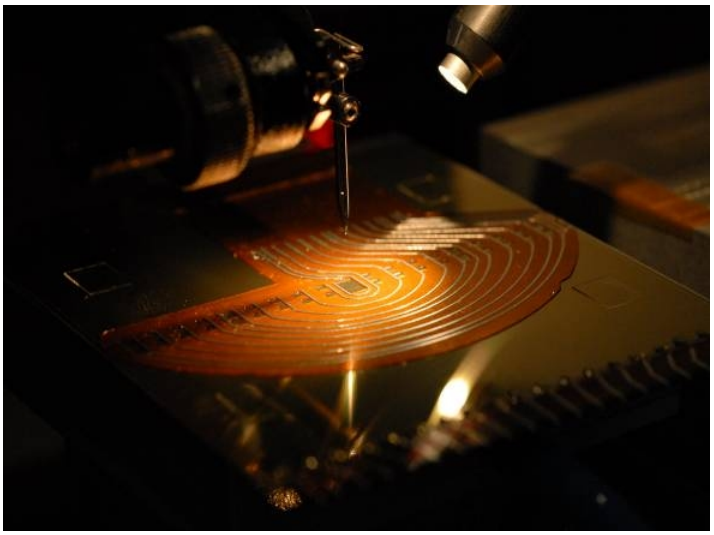

With the same technology as by wrap-arounds we bonded the transition cable on the detector.

8. **bonds passivation**

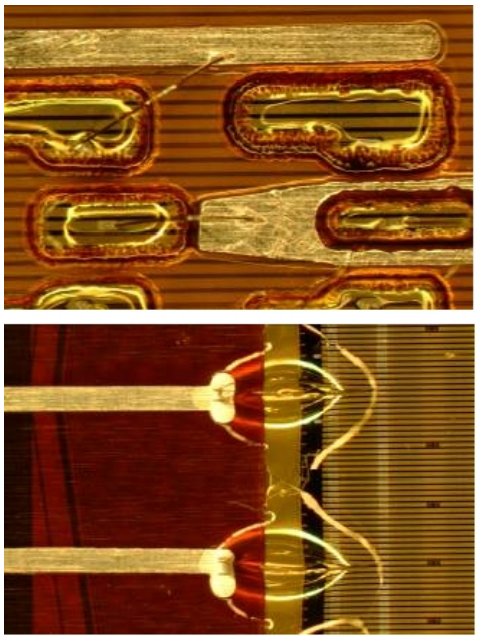

Aluminum wire and it's bonds are very fragile so it is necessary to fix bonds. We fixed bonds by the same glue - passivated. On the picture higher we see passivated bonds by a transition cable and on the picture lower by a wrap-around cable.

A The Basics of Wire Bonding

Wire bonding is an electrical interconnect technology developed by microelectronics industry and today used excessively in (solid state) detector construction. It allows to interconnect electronic chips, printed circuit boards, pitch adapters and solid state sensors (usually silicon).

A basic ingredient, common to most bonding methods is the transfer of ultrasonic energy via the resonating bond tool to the interface between the bond wire and the bond pad in order to form a metallurgical bond, a kind of micro weld.

An excellent introduction to the topic is provided by G. Harman: Wire bonding in Microelectronics, McGraw-Hill, 2nd edition (1996)

Overview of the different bonding methods

Generally one distinguishes between *wedge* and *ball* bonding technologies

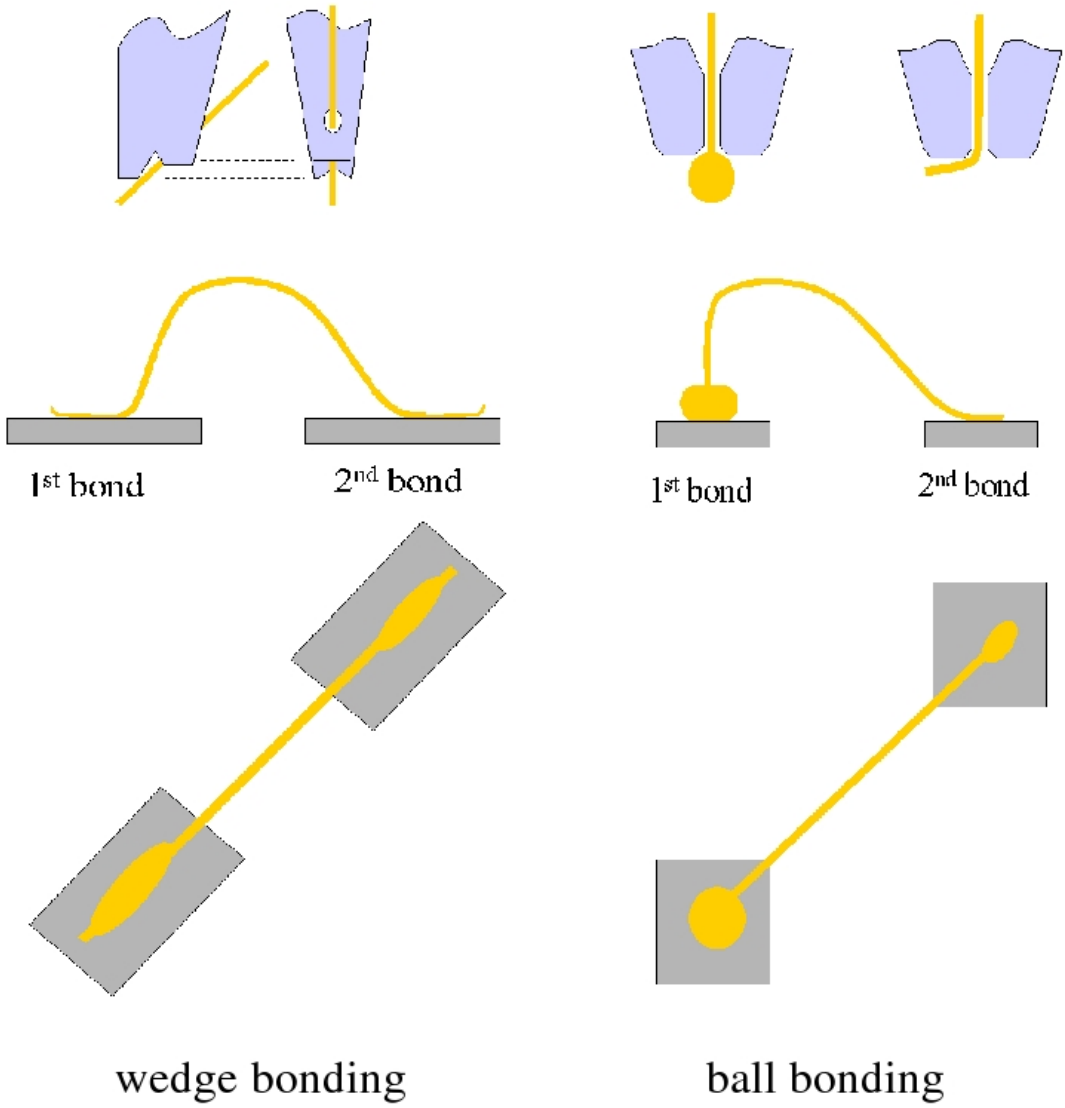

The bond tools (upper part of schematics) and the way the wire is held are very different. The orientation of the wedge tool (left schematic) defines the bond direction. The bond head

of a wedge bonder must therefore be oriented in a straight line from the 1st to the 2nd bond, before the 1st bond can be made. This requires a more complex rotating bond head than for ball bonders (right schematic), where the wire can be bent and drawn from the first bond in any direction. The heavier mechanics and the more complex bond head movement slow down the wire bonding process. In ball bonding the first bond is made by means of a ball which is formed before be means of an electrical spark, while the second bond resembles a wedge bond.

Currently the DSF bondlab is performing exclusively *Ultrasonic wedge bonding with Aluminum wires*. For completeness we give a brief historical overview of the different bonding technologies.

Thermocompression (TC) bonding. Developed in 1957 for gold wire on gold gold pads, but practically not in use anymore. As there is no ultrasonic energy involved, it requires a combination of high temperature (¿300C) and high force at the bond interface.

Ultrasonic (US) wedge bonding has been used in microelectronics industry since about 1960, mainly for device production, but was there later replaced by thermosonic gold ball bonding (see below). In High Energy Physisics (HEP) applications, US wedge bonding is the predominant method, as it doesn't require any substrate heating and therefore is very versatile. US wedge bonding is mainly used to bond Al wires (diameter in the range 17 - 75 um and even over 0.5mm in special cases!) to Al or Au bond pads. Following sequence of pictures shows a complete wedge bonding sequence (in a very schematic way).

1. 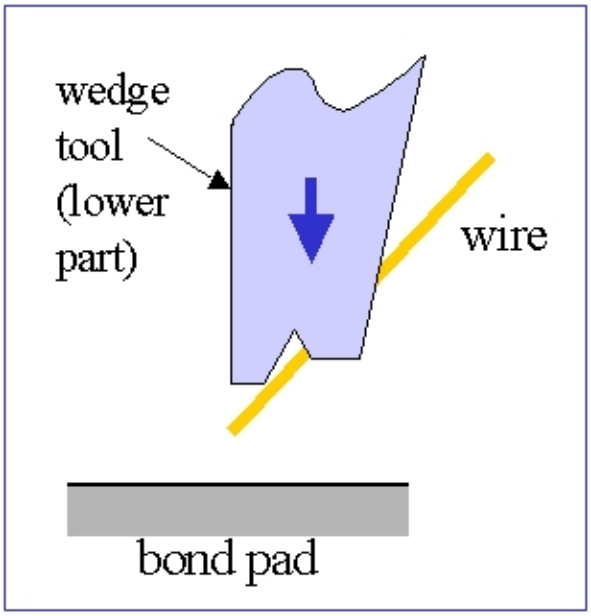

2.

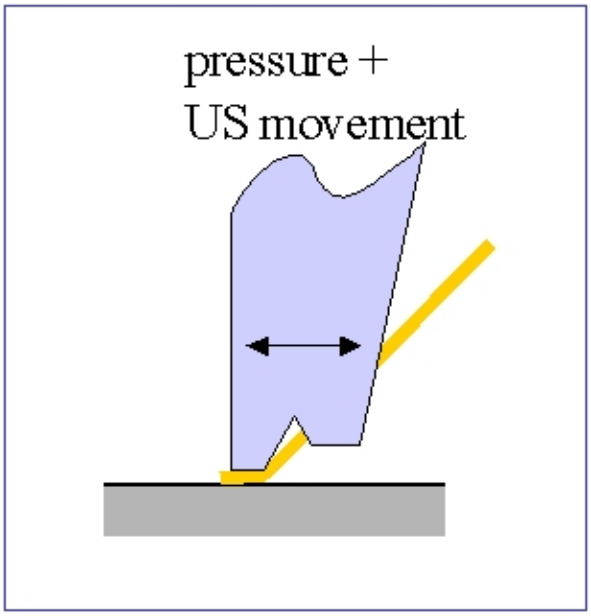

3.

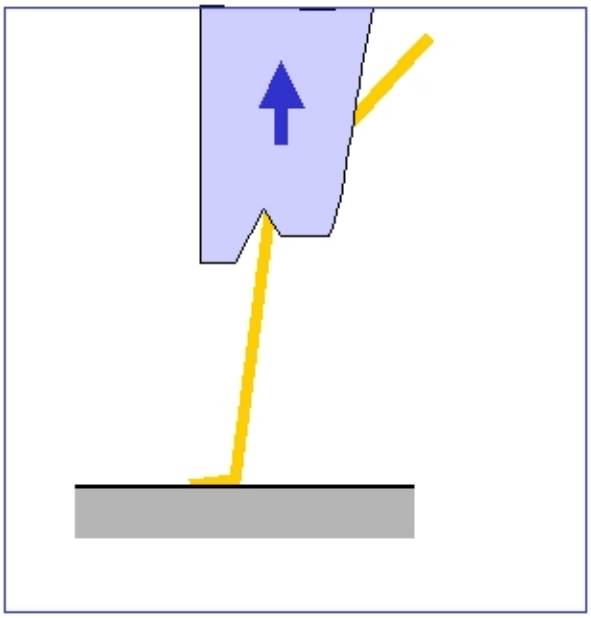

4. 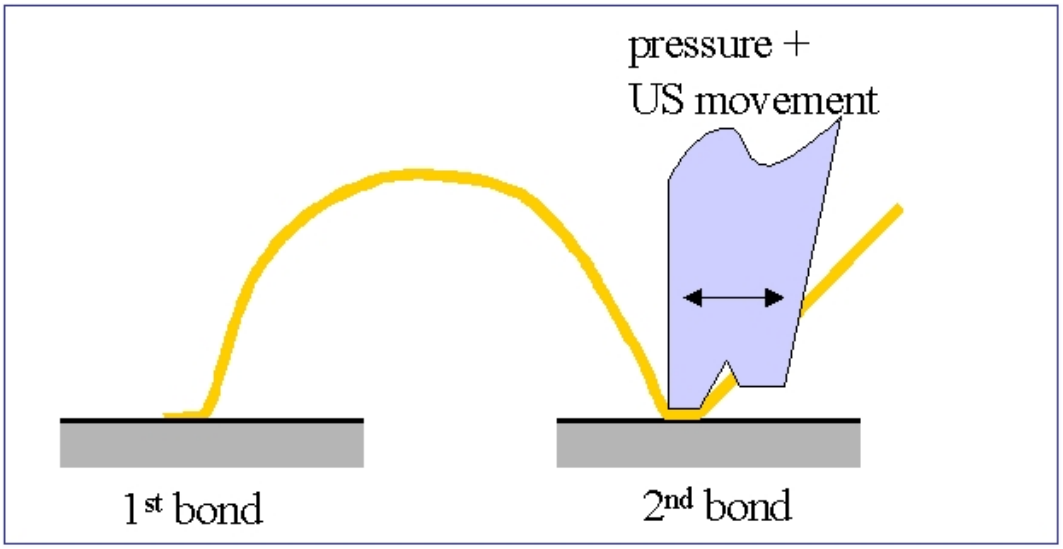

5. 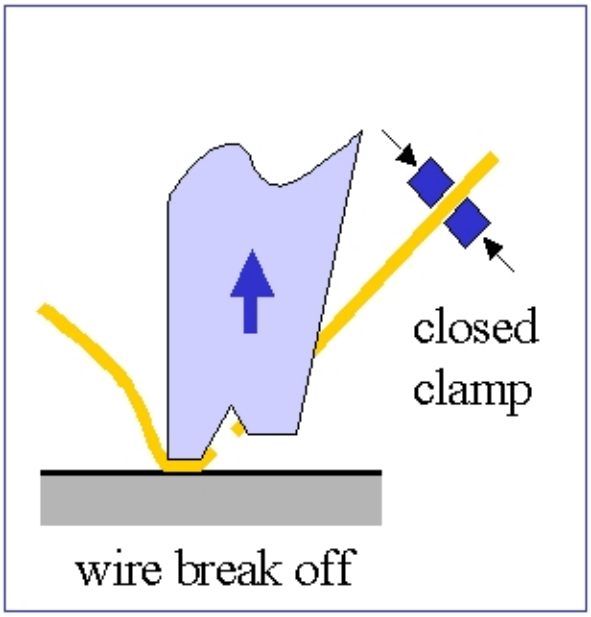

Thermosonic (TS) gold ball bonding was introduced in 1970 and is today widely used in industry, mainly for packaging chips. Compared with TC, the ultrasonic activation allows to lower the interface temperature to 125-220C.

Reference

[1] CARMINATI, F. FOKA, P. GIUBELLINO, P. MORSCH, A. REVOL, J. P. ŠAFAŘÍK, K. SCHUTZ, Y. WIEDEMANN, U. A., *ALICE, Physics Performance Report, Volume I.*, CERN/LHCC: ALICE PPR Volume I. 2003

[2] ALICE team, *ALICE - Technical Design Report of the Inner Tracking System*, CERN: CERN/LHCC. June 1999

[3] LOURENÇO, CARLOS, *Heavy Ion Collisions at the LHC: The Alice Experiment* CERN, Geneva, Switzerland: arXiv:hep-ph/9612221 v1 1 Dec 1996

[4] BONVINICI, V. BURGER P., GREGORIO, A. RASHEVSKY, A. VACCHI, A. ZAMPA, N., *Characterising large area silicon drift detectors wit MOS injectors*, EDITRICE COMPOSITORI BOLOGNA, Bologna, Italy, 1999, Il Nuovo Cimento - Vol. 112 A, N. 1-2, 1999, p. 137-146

[5] http://ssd-rd.web.cern.ch/ssd-rd/bondlab/wirebonding/Bonding_basics.htm

[6] http://extra.ivf.se/ngl/A-WireBonding/ChapterA.htm